# Fracture and mechanical properties of $MoSi_2$ and $MoSi_2$+SiC

J. Dusza[1]*, P. Hvizdoš[2]

[1] *Institute of Materials Research of the Slovak Academy of Sciences, Watsonova 47, 043 53 Košice, Slovak Republic*
[2] *Este IB, Universitat Politécnica de Catalunya, Dept. of Mater. Sci. & Metallurg. Eng. Diagonal 647, 08028 Barcelona, Spain*

Received 21 April 2006, received in revised form 21 September 2006, accepted 4 October 2006

**Abstract**

The mechanical properties as hardness, bending strength, fracture toughness, and creep of a monolithic molybdenium disilicide and a $MoSi_2$+SiC composite have been investigated. The bending strength was measured in four-point bending, the fracture toughness using single edge V-notched specimens at room temperature. The creep experiment was carried out in four-point bending mode in the temperature range from 1100 °C to 1200 °C in air. The influence of high-temperature heat treatments in air at 1400 °C and 1550 °C for 100 h on the bending strength of $MoSi_2$ at room temperature has been investigated, too.

The hardness and fracture toughness of $MoSi_2$+SiC composites were slightly improved by the incorporated SiC particles into the $MoSi_2$ matrix. The strength values of composites were relatively low because of the presence of defects in their microstructure. The creep resistance of $MoSi_2$+20vol.%SiC composite was significantly improved in comparison with the monolithic $MoSi_2$. Heat treatment at 1400 °C had no influence on the strength but a heat treatment at 1550 °C significantly decreased the strength due to the formation of large pores in the bulk of the material.

K e y w o r d s: $MoSi_2$, microstructure, fracture, mechanical, properties

## 1. Introduction

Recently, there is an increasing need for structural materials that can withstand oxidizing environments at elevated temperatures up to 1500 °C. Such materials are important for modifications in energy production technologies with the aim to improve their efficiency and to reduce carbon dioxide exhaust level. Similarly, advanced aircraft engine designs require new materials that can operate at temperatures higher than those tolerable for superalloys. Materials based on $MoSi_2$ are promising candidates for wide variety of elevated temperature structural applications thank to their high melting point (2030 °C), excellent oxidation and corrosion resistance, and high temperature ductility above the brittle-ductile transition temperature in the vicinity of 1000 °C [1–4]. However, the main disadvantage, limiting their use, is the low fracture toughness at lower temperatures (< 1000 °C) and the low strength and creep resistance at high temperatures. In order to improve the mentioned properties, various approaches based on incorporating of SiC, Nb and $ZrO_2$ particles or SiC whiskers into the matrix have been used [5–10]. The highest fracture toughness was reported for the $MoSi_2$ reinforced by refractory metal wires, with "graceful failure" fracture morphology. Reinforcing of $MoSi_2$ by tantalum particles leads to a significant toughening due to the plastic deformation of ductile Ta particles bridging the crack opening. However, the refractory metal reinforcement in $MoSi_2$-based composites can result in reaction and oxidation problems. Similarly as in the oxide structural ceramics, the transformation toughening effect has been utilized in the $ZrO_2$ particle – $MoSi_2$ matrix composites. Unstabilized $ZrO_2$ tetragonal-to-monoclinic martensitic phase transformation occurs above the brittle-to-ductile transition temperature of the $MoSi_2$, where the $MoSi_2$ is still ductile. The expansional volumetric strain originated with this transformation leads to a dislocation formation in the $MoSi_2$ with positive effect on the fracture toughness of the material.

*Corresponding author: tel.: +421 557922462; fax: +421 557922408; e-mail address: jdusza@imr.saske.sk

The brittle-to-ductile transition temperature can be reduced by high temperature pre-strain, surface films and internal interfaces. The plasticity enhancement by high temperature pre-strain is enabled by injection of dislocations into the dislocation density limited material and by activation of dislocation sources not available in material prior the pre-strain. However, it is important to note, that the plasticity enhancement was observed in compression and indentation testing only.

Fracture toughness improvement was achieved in $MoSi_2$+SiC composite by activating different toughening mechanisms as crack deflection or crack bridging. However, the fracture strength has not been improved due to the presence of SiC clusters in the material.

The elevated temperature creep behaviour of polycrystalline $MoSi_2$ is sensitive to grain size. This dependence is characterized by a grain size exponent in the range of 5–8 [11]. The addition of the SiC particles to the $MoSi_2$ increases its creep resistance in spite of the fact that the addition leads to decrease of the $MoSi_2$ grain size. The creep mechanisms in $MoSi_2$--based materials appear to be a combination of dislocation glide/climb together with grain boundary sliding.

During the recent years new processing techniques have been applied to prepare $MoSi_2$+SiC composites, such as reactive sintering and reactive hot pressing [12, 13]. A moderate increase in fracture toughness values and significant increase in the high temperature compressive yield strength have been achieved due to the addition of SiC reinforcements.

The aim of the present work was to study and compare the fracture and mechanical properties of monolithic $MoSi_2$ and $MoSi_2$+SiC composite in bending and to investigate an influence of the SiC particles on the creep mechanisms in the temperature range 1100–1200 ℃ in air.

## 2. Experimental

The materials used in this investigation were monolithic $MoSi_2$ and $MoSi_2$+20vol.%SiC, prepared by Cesiwid, Erlangen, Germany. Specimens for bending creep tests were cut to the dimensions 3 × 4 × 45 $mm^3$ and polished with 15 $\mu$m finish on their tensile surface. The $MoSi_2$ was studied in as-received as well as in heat-treated form. Heat treatment of the bend bars with dimensions 3 mm × 4 mm × 45 mm and with a 15 $\mu$m finish on the tensile surface was carried out at 1400 ℃/100 h and 1550 ℃/100 h in air [14, 15].

Samples for microstructure analysis were prepared using standard procedure and investigated using optical microscopy, as well as scanning and transmission electron microscopy (SEM and TEM). The volume fraction of individual phases (pores) was measured using an image analyser and statistical methods. X-ray microanalysis (EDX) was used for identification of individual phases present in the microstructure.

Thin foils of the as-received materials and of the tensile surfaces of the crept specimens were prepared for the microstructure and substructure observations which were carried out using TEM techniques in order to identify the high temperature deformation mechanisms.

Bend test specimens with dimension 3 × 4 × 45 $mm^3$ were used for the bending strength (height = 3 mm) and fracture toughness measurement (height = 4 mm). The specimens were tested in four-point flexure with spans of 40 mm and 20 mm at room temperature at a loading rate of 0.5 mm/min. The measured bending strength values were evaluated using Weibull statistics. For the fracture toughness measurement the sharp notch was introduced according to the VAMAS TWA#3/ESIS TC6 Round Robin Instruction using a razor blade [16]. In all cases the notch tip radius was less than 10 $\mu$m. The values of $K_{IC}$ were computed using the formula [17]

$$K_{IC} = \sigma a^{1/2} Y = \frac{3}{2} F_f \frac{S_1 - S_2}{B W^{1.5}} \frac{\sqrt{\alpha}}{(1-\alpha)^{1.5}} Y, \qquad (1)$$

$$Y = 1.9887 - 1.326\alpha - \frac{(3.49 - 0.68\alpha + 1.35\alpha^2)\alpha(1-\alpha)}{(1+\alpha)^2}, \qquad (2)$$

where $\sigma$ is the fracture stress, $F_f$ is the fracture load, $B$ and $W$ are the specimen thickness and height, respectively, $S_1$ and $S_2$ are the outer and inner support spans and $\alpha = a/W$, where $a$ is the crack's depth.

The creep tests were carried out in the four-point bending mode with inner/outer roller spans 20/40 mm. The bending bars were tested at temperatures from 1100 to 1200 ℃ under loads from 20 to 100 MPa. The tests were realized in a creep furnace with a dead weight loading system in air. From specimen deflection data, measured by two inductive transducers between the centre and the inner roller and collected by a computer data acquisition system, the outer fibre strain was calculated and recorded. The accuracy of the deflection measurement was approximately ± 1 $\mu$m. The creep experiments at all stress/temperature combinations were carried out up to 1 % bending strain.

From the deflection data, the outer fibre strain was calculated as a function of time, $t$, by the method of Hollenberg et al. [18] and taken as the creep strain, $\varepsilon$. The creep rate was calculated from the slope of the $\varepsilon$ versus $t$ curve. The steady-state creep rate, $\dot{\varepsilon}$ , is usually described by the Norton equation:

$$\dot{\varepsilon} = A\sigma^n \frac{1}{d^m} \exp\left(-\frac{Q_C}{RT}\right), \qquad (3)$$

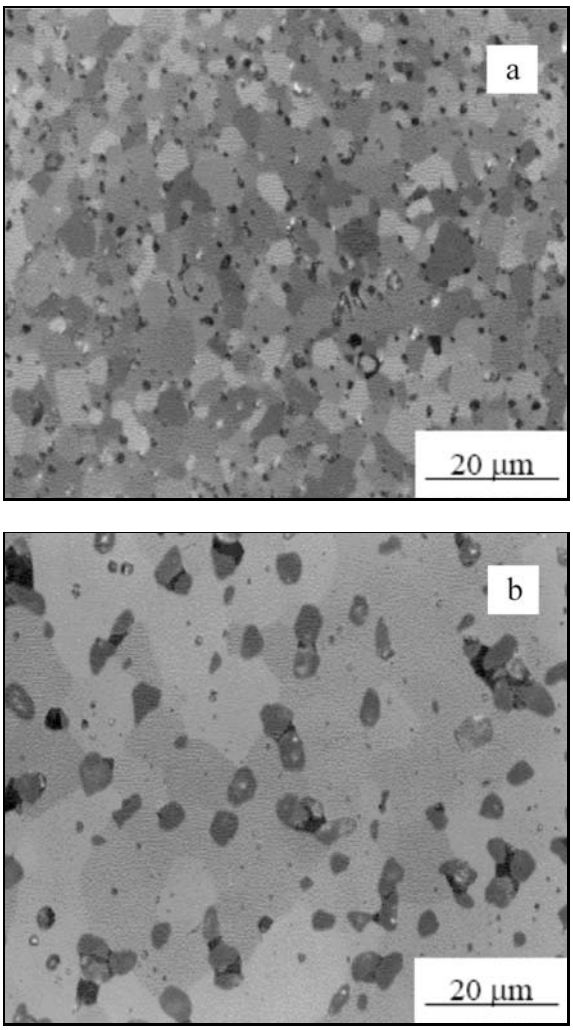


Fig. 1. Microstructure of the investigated materials in cross-polarized illumination: (a) monolithic $MoSi_2$, (b) $MoSi_2$+SiC.

where $A$ is a constant, depending on the respective material and on its microstructure, $\sigma$ is the stress, $n$ is the stress exponent, $d$ is the grain size, $m$ is the grain size exponent, $Q_C$ is the activation energy for creep, and $T$ and $R$ have their usual meaning.

After the bending strength test and fracture toughness test, macro- and microfractography have been used with the aim to identify and characterize the strength degrading defects and the toughening mechanisms [19].

## 3. Results and dicussion

### 3.1. Microstructure characteristics

Microstructures of the studied materials are shown in Fig. 1a,b. Using SEM and EDX it was found that there were three different phases present in the microstructure of the monolithic $MoSi_2$: matrix $MoSi_2$ grains, $SiO_2$ and a little of $Mo_5Si_3$ (hexagonal Nowotny phase). TEM observations of the as-received materials proved that silica ($SiO_2$) particles were frequently present in the triple grain junctions of $MoSi_2$ grains and occasionally were placed intragranularly, inside the $MoSi_2$ grains. The mean grain size of $MoSi_2$ was approximately 7 $\mu$m. The silica particles were usually spherical with diameter of the intergranular particles in the range from 1 to 5 $\mu$m and the intergranular ones with diameter from 0.2 to 2 $\mu$m. TEM was used to determine whether there was any amorphous phase present at the grain boundaries. It was found that the grain boundaries were clear and the $SiO_2$ did not wet the matrix boundaries. The composite material, beside the features found also in the monolithic material, contained SiC grains with average size of 5 $\mu$m, clusters of grains and porosity of 3.2 vol.%. The $MoSi_2$ matrix grains were larger than those in the monolithic material and typically had dimensions from 10 to 15 $\mu$m.

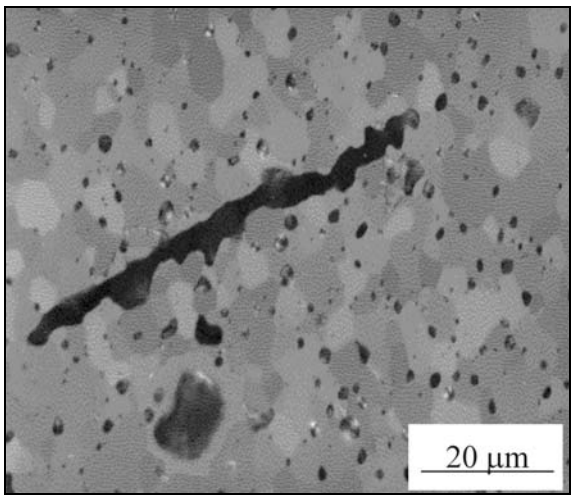


Fig. 2. Crack-like pore in the microstructure of the sample heat treated at 1550 ℃/100 h.

The microstructure of the material heat-treated at 1400 ℃/100 h is very similar to that of the as-received material, apart from a continuous $SiO_2$ layer on the surface of the heat treated samples with a thickness approximately 10 $\mu$m. The microstructure of the material heat treated at 1550 ℃/100 h is significantly different from the as-received one. Pores with both a spherical shape and with a crack-like shape have been observed, Fig. 2. The size of the spherical pores was up to 50 $\mu$m and that of the elongated pores up to 200 $\mu$m, and they are often filled with silica. Similarly, continuous $SiO_2$ layers with an average width of 15 $\mu$m have been found on the external surface of material heat-treated at 1550 ℃/100 h.

Table 1. Mechanical properties of the investigated materials

| | Mean strength (MPa) | Weibull parameters | | $K_{IC}$ (MPa·m$^{1/2}$) | HV (GPa) |
|---|---|---|---|---|---|
| | | $\sigma_0$ (MPa) | $m$ | | |
| $MoSi_2$ | 251 | 276 | 4.62 | 3.4 | 9.9 |
| $MoSi_2$+20%C | 156 | 162 | 12.9 | 3.7 | 11.2 |

### 3.2. Room temperature mechanical properties

The room temperature mechanical properties are illustrated in the Table 1. According to the results, the mean strength of the monolithic material and composite is 251 MPa and 156 MPa, respectively. The characteristic strength for the monolithic material is 276 MPa and the Weibull modulus is 4.62. The characteristic strength of the composite is even lower, 162 MPa, but the Weibull modulus is higher, 12.9, comparing to the $MoSi_2$. The mean value of the fracture toughness of the $MoSi_2$ is 3.4 MPa·m$^{0.5}$ and of the composite 3.7 MPa·m$^{0.5}$. The hardness of the monolithic material was found to have a value of 10.5 GPa and of the composite 12.6 GPa.

The low bending strength can be explained by the low fracture toughness and by the presence of relatively large defects in both investigated materials. Fractography revealed that the characteristic strength degrading defects in the monolithic material are pores, clusters of pores and clusters of $SiO_2$ with an average size of 60 $\mu$m and in the composite material clusters of SiC grains with an average size of 50 $\mu$m, Fig. 3. The frequency of the occurrence of defects in monolithic materials is lower comparing to the situation in composite material. This is the reason of the higher average strength of the monolithic material and also the reason of the higher Weibull modulus of the composite.

The fracture toughness of the investigated materials is low, lower as the characteristic ceramics on the base of silicon nitride. The composite exhibits slightly higher toughness, which can be explained by the toughening mechanisms of crack deflection at SiC grains, occurring during the crack propagation in this material, as it was observed by fractography of fracture path.

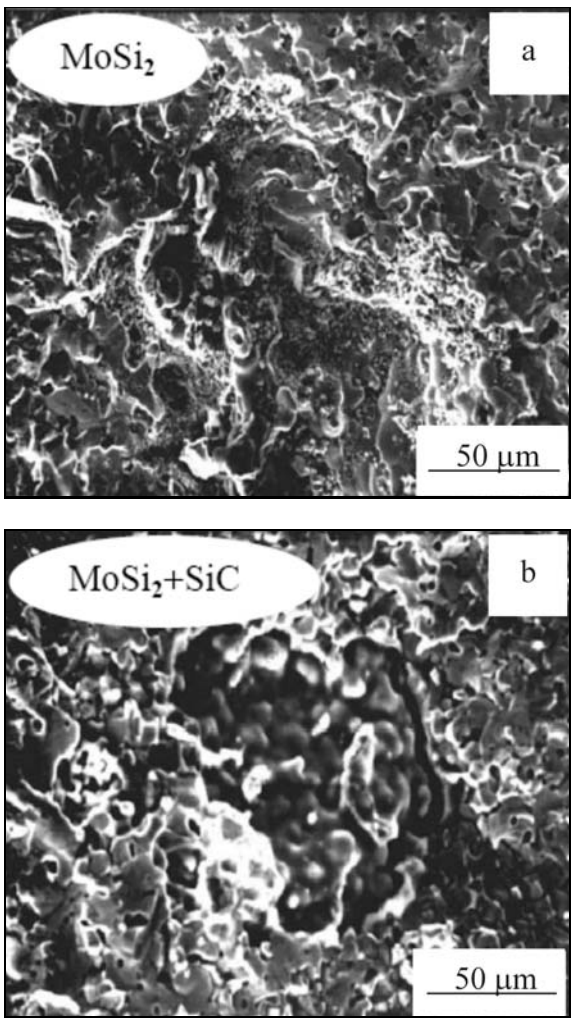


Fig. 3. Fracture origins in the as-received $MoSi_2$ (a) and composite (b).

### 3.3. Effect of the heat treatment/oxidation on the strength

The results of the four-point bend tests are summarized in Table 2 and Fig. 4. The heat treatment at 1400 ℃/100 h has no influence on the Weibull parameters of $MoSi_2$ and the mean strength and Weibull modulus are approximately 250 MPa and 11 for as-received and heat-treated material. Such a Weibull modulus is characteristic for monolithic structural ceramics, which exhibits a relatively high scatter in its strength properties. Different results have been found after heat treatment at 1550 ℃/100 h. The mean strength is approximately 30 % lower than in the as-received condition, whereas the Weibull modulus is significantly higher. Because advanced structural materials should not only exhibit a high Weibull modulus but also high strength, the increase in Weibull modulus is outweighed by the decrease in strength. As it was mentioned before, fractographic study of

Table 2. Strength and Weibull parameters of the investigated materials in as-received and heat-treated form

| | As-received | | | 1400 °C/100 hours | | | 1550 °C/100 hours | | |
|---|---|---|---|---|---|---|---|---|---|
| | Mean strength (MPa) | Weibull parameters | | Mean strength (MPa) | Weibull parameters | | Mean strength (MPa) | Weibull parameters | |
| | | $\sigma_0$ (MPa) | $m$ | | $\sigma_0$ (MPa) | $m$ | | $\sigma_0$ (MPa) | $m$ |
| $MoSi_2$ | 251 | 278 | 4.62 | 253 | 264 | 11.0 | 179 | 181 | 17.5 |
| $MoSi_2$+20%SiC | 156 | 162 | 12.9 | – | – | – | 152 | 158 | 11.3 |

the fracture surface of specimens after four-point bend testing showed that approximately 15 % of the as-received specimens failed from large volume defects in the form of pores, clusters of pores or clusters of pores accompanied by a cluster of $SiO_2$ phase. These defects were located close to the tensile surface or edges of the bend bars. In the remaining specimens, the fracture origins could not clearly be identified and these probably were surface defects with a smaller size. Very similar results have been found for the material heat treated at 1400 °C/100 h. On the other hand, fractography of the failed bend bars heat-treated at 1550 °C/100 h showed that in all the specimens the fracture origin was a large defect of very uniform features. These defects were surface or subsurface defects in the form of pores or crack-like voids, often filled with $SiO_2$ phase, which probably arose during the heat treatment at 1550 °C/100 h. The size of these defects varied from 80 $\mu$m to 200 $\mu$m with an approximately elliptical shape on the fracture surface, Fig. 5.

The material heat-treated at 1400 °C/100 h behaves according to the literature data. The continuous $SiO_2$ layer protects the underlying $MoSi_2$ against further oxidation and no changes in the microstructure of the bulk of the material occur. No other phases have been found between the $MoSi_2$ and $SiO_2$ layers. The defect population seems to be similar to that of the material in the as-received condition, which is also confirmed by the results of the strength tests.

The strength difference between the as-received samples and samples heat-treated at 1550 °C/100 h can be explained by the presence of new, larger defects located at or near the surface of the bend bars. These defects are responsible for the decrease of the mean strength according to the Griffith relation and their similarity in terms of their size, shape, location and orientation is responsible for the increase in Weibull modulus. They can arise during the heat treatment in two possible ways: as the result of oxidation or as the result of changes in the bulk material. A detailed examination of the cross-section of samples heat-treated at 1550 °C/100 h revealed that such large defects are found throughout the bulk material and that they are occasionally present at or near the surface. This suggests that they form as bulk defects during the heat

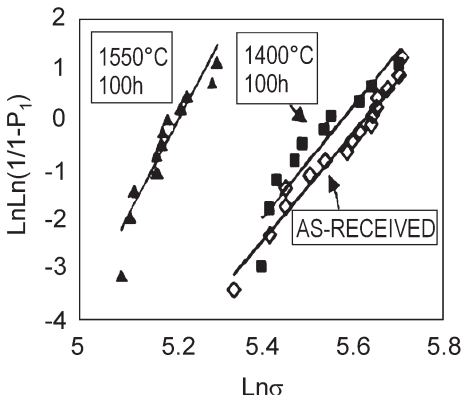


Fig. 4. Weibull plot of the strength data of as-received and heat-treated $MoSi_2$.

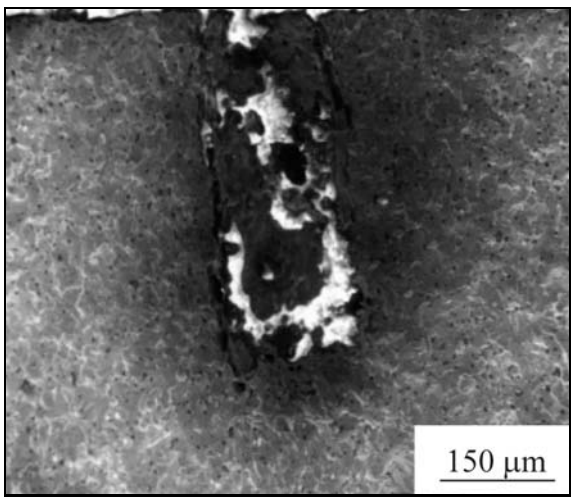


Fig. 5. Defect as a fracture origin in the heat-treated $MoSi_2$ at 1550 °C/100 h.

treatment by coalescence of pores already present in the as-received material. The nuclei of the large defects are probably the larger pores already present in the as-received material. Microstructure investigations suggest two mechanisms of pore coalescence, Fig. 6. Large globular pores grow from separated pre-existing

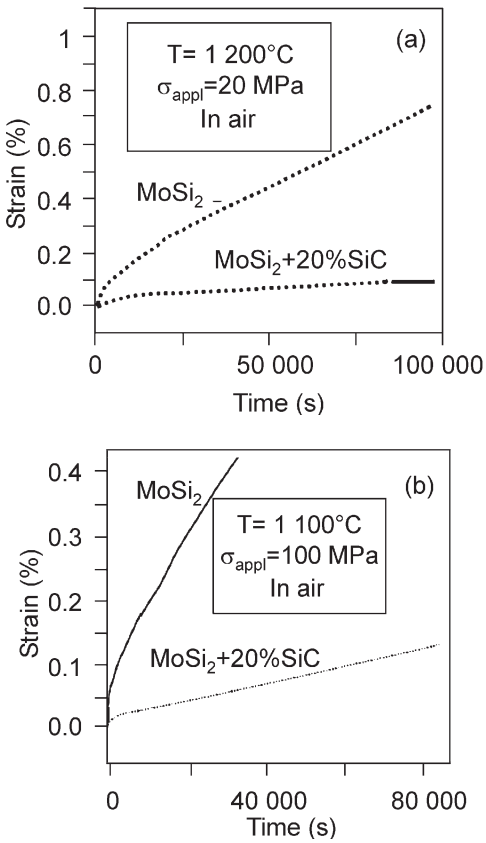


Fig. 6. Comparison of the creep behaviour of the studied materials at 1100 °C (a) and 1200 °C (b).

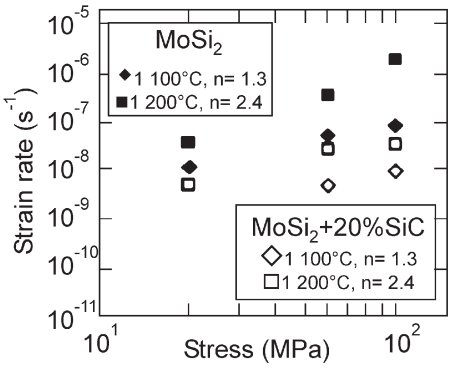


Fig. 7. Minimum creep rates as functions of applied stresses. Determining the stress exponents.

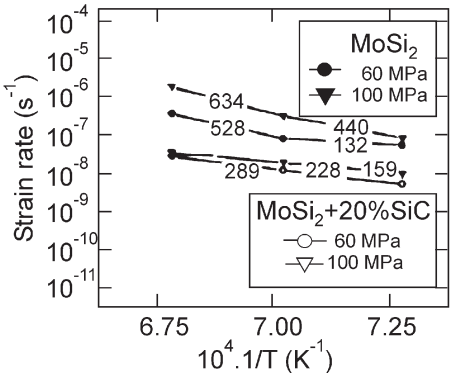


Fig. 8. Arrhenius plot for the studied materials. Calculation of the apparent activation energies for creep.

larger pores surrounded by a uniform distribution of smaller pores. On the other hand, elongated pores result from the coalescence of originally closely spaced larger pores. The driving force for this mechanism is the lower surface energy of the large pores in the bulk material after the heat treatment at 1550 °C/100 h. In the four-point bend test these defects act as sites to initiate fracture, causing the strength degradation.

### 3.4. Creep behaviour

The creep tests showed a remarkable difference between the creep behaviour of both materials, as can be seen from Fig. 6. At the test condition of 1100 °C/100 MPa the monolithic $MoSi_2$ exhibited strain of 0.15 % after a loading time of 2 hours, while the $MoSi_2$+20%SiC composite showed the same level of strain after more than 20 hours.

At the testing conditions of 1200 °C/20 MPa the strain in the monolithic $MoSi_2$ had a value of approx. 0.6 % after 20 hours, while the composite had less than 0.1 % at the same conditions, Fig. 6b.

Figure 7 shows the creep rates as a function of applied stresses for both monolithic and composite materials at three different testing temperatures together with the calculated creep exponents. The values of the creep exponents are similar for both materials, about 1.75. However, they are lower in comparison with $MoSi_2$ composites reinforced with 20 % SiC whiskers [11].

The apparent activation energies calculated from the Arrhenius plots are given in Fig. 8. The apparent activation energy of the monolithic $MoSi_2$ at the low applied stress had a value of approximately 250 kJ/mol, which is in good agreement with the activation energy for diffusion of silicon in $MoSi_2$ [20]. The apparent activation energy at the highest applied stress (100 MPa) was 634 kJ/mol which, in combination with the stress exponent value about 2.4, suggests a change in the creep controlling mechanism, which in this case was probably dislocation climb [21]. This fact is also supported by TEM observations of the samples after creep testing, where a large number of dislocations in the $MoSi_2$ grains have been found, Fig. 9. The lower creep rate in the case of $MoSi_2$+SiC composite can be explained by the different $SiO_2$ content in the monolithic and composite $MoSi_2$, and by the presence of the SiC grains in the microstructure of the composite.

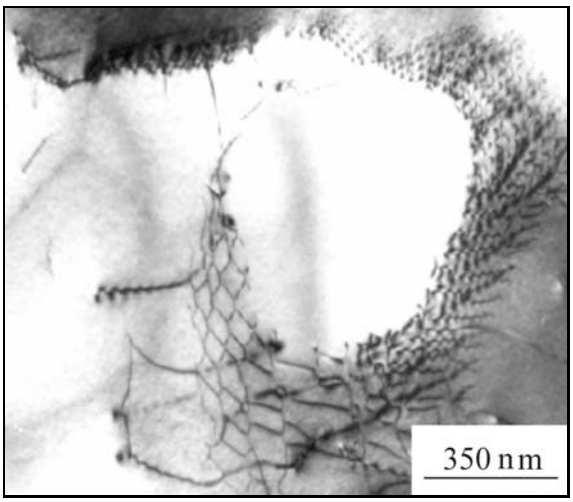


Fig. 9. Dislocation networks in $MoSi_2$ grain.

According to Sadananda et al. [11] the creep behaviour (creep rate) of polycrystalline $MoSi_2$ is very sensitive to grain size and is controlled primarily by dislocation glide/climb, as well as by grain boundary sliding accommodated by dislocation plasticity. The grain size exponent for $MoSi_2$ was found to be in the range of 5–8, which is higher than expected for Nabarro-Herring creep (grain size exponent of 2) and Coble creep (grain size exponent of 3). For $MoSi_2$+SiC composites it was found that in the case of volume fraction of SiC particles from 5 % to 20 % the creep rate was higher than that of unreinforced $MoSi_2$, while creep rates of composite reinforced with 40 % SiC particles were substantially lower. This behaviour was found to be related to the fact, that with increasing SiC addition the grain size of the $MoSi_2$ matrix is reduced, promoting grain boundary sliding.

In the materials studied in the present investigation the grain size of the $MoSi_2$ in $MoSi_2$+SiC composite is significantly larger in comparison with the grain size of monolithic $MoSi_2$. This mere fact itself is an explanation for the improved creep resistance. Furthermore, the presence of SiC particles on the grain boundaries of $MoSi_2$ probably modifies the geometry and chemical composition of the silica phase in the composite resulting in a substantially higher creep resistance in comparison with the $MoSi_2$.

## 4. Summary

– The strength of the monolithic $MoSi_2$ and $MoSi_2$+20%SiC is low due to the present defects in the microstructure of the materials in the form of pores, clusters of pores and clusters of SiC particles;

– the incorporation of the SiC particles into the $MoSi_2$ matrix slightly increased the hardness, because of the higher hardness of the SiC and the fracture toughness due to the reinforcing mechanisms as crack deflection;

– the high-temperature heat treatment in air at 1550 ℃ for 100 h leads to a significant strength degradation of the $MoSi_2$. This is caused by the formation of large pores by a pore coalescence mechanisms in the volume (statistically also near the surface) of the samples and not by an oxidation-induced degradation of the surfaces;

– $MoSi_2$+20%SiC composite exhibited an excellent creep resistance in the temperature range of 1100–1200 ℃ with the creep deformation rate almost one order lower than that of the monolithic $MoSi_2$. The creep of $MoSi_2$ appears to be controlled primarily by dislocation glide/climb as well as grain boundary sliding accommodated by dislocation plasticity. The grain boundary sliding in the composite is significantly suppressed due to the higher grain size and by the presence of SiC particles on the $MoSi_2$ grain boundaries.

## Acknowledgements

The work was supported in part by the NANOSMART, Centrum of Excellence of SAS, Slovak Grant Agency for Science via grant No. 2/4173/04 and by the Science and Technology Assistance Agency under the contract No. APVT-51–049702.

We thank K. Kromp and W. Heider for fruitful discussions and the supply of experimental material.

## References

[1] VASUDEVAN, A. K.—PETROVIC, J. J.: Mater. Sci. Eng. A, *155*, 1995, p. 1.
[2] SHAW, L.—MIRACLE, D.—ABBASCHIAN, R.: Acta Metal. Mater., *43*, 1995, p. 4267.
[3] COSTA E SILVA, A.—KAUFMAN, M. J.: Mater. Sci. Eng. A, *195*, 1995, p. 75.
[4] MALOY, S.—HEUER, A. H.—LEWANDOWSKI, J.—PETROVIC, J. J.: J. Am. Ceram. Soc., *74*, 1991, p. 2704.
[5] PETROVIC, J. J.—VASUDEVAN, A. K.: Mat. Sci. Eng. A, *261*,1999, p. 1.
[6] JAYASHANKAR, S.—KAUFMAN, M. J.: Scripta Met. Mater., *26*, 1992, p. 1245.
[7] YAMADA, T.—HIROTA, K.—YAMAGUCHI, O.—ASAI, J.—MAKAYAMA, Y.: Mater. Res. Bulletin, *7*, 1995, p. 851.
[8] BHATTACHARYA, A. K.—PETROVIC, J. J.: J. Am. Ceram. Soc., *75*, 1992, p. 23.
[9] SOBOYEJO, W.—BROOKS, D.—CHEN, L. C.: J. Am. Ceram. Soc., *78*, 1995, p. 1481.
[10] PETROVIC, J. J.: Mat. Sci. Eng. A, *192/193*, 1995, p. 31.
[11] SADANANDA, K.—FENG, C. R.—JONES, H.—PETROVIC, J. J.: Mater. Sci. and Eng. A, *155*, 1992, p. 227.

[12] AIKIN, R. M.: J. Ceram. Sci. Proc., *12*, 1991, p. 1643.
[13] NIIHARA, K.—SUZUKI, Y.: Mat. Sci. Eng. A, *26*, 1999, p. 6.
[14] DUSZA, J.—STEINKELLNER, W.—KROMP, K.—STEEN, M.: Mat. Sci. Eng. A, *259*, 1999, p. 149.
[15] BALLÓKOVÁ, B.—LOFAJ, F.—DUSZA, J.—KROMP, K.—STEINKELLNER, W.: Praktische Metallog., *30*, 1999, p. 523.
[16] KÜBLER, J.: VAMAS TWP#3 / ESIS TC6 round robin on fracture toughness of ceramics using the SEVNB method. Dübendorf, Switzerland, EMPA 1997.
[17] SRAWLEY, J. E.—GROSS, B.: Cracks in Fracture. Am. Soc. Test. Mater., Spec. Tech. Publ., No. 601, Philadelphia, PA, ASTM 1976, p. 559.
[18] HOLLENBERG, G. W.—TERWILLINGER, G. R.—GORDON, R. S.: J. Am. Ceram. Soc., *54*, 1971, p. 196.
[19] DUSZA, J.—STEEN, M.: International Materials Reviews, *44*, 1999, p. 165.
[20] KOFSTAD, P.: In: High Temperature Oxidation of Metals. New York, Wiley 1966.
[21] DUSZA, J.—HVIZDOŠ, P.—STEINKELLNER, W.—KROMP, K.: Scripta Materialia, *37*, 1997, p. 471.